Muons and Radioactive Ions as Quantum Sensors

Iain McKenzie

What properties does a system need to be considered a quantum sensor?

(1) The quantum system has discrete, resolvable energy levels.
(2) It must be possible to initialize the quantum system into a well-known state and to read out its state.
(3) The quantum system can be coherently manipulated, typically by time-dependent fields.
(4) The quantum system interacts with a relevant physical quantity, such as an electric or magnetic field.

C.L. Degen, F. Reinhard, and P. Cappellaro, *Rev. Mod. Phys.* **89**, 035002 (2017)

(1) The quantum system has discrete, resolvable energy levels.

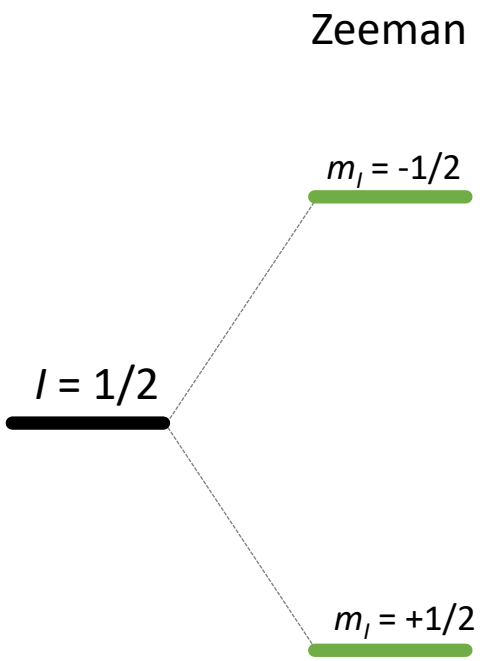

Mu^+

τ = 2.2 µs

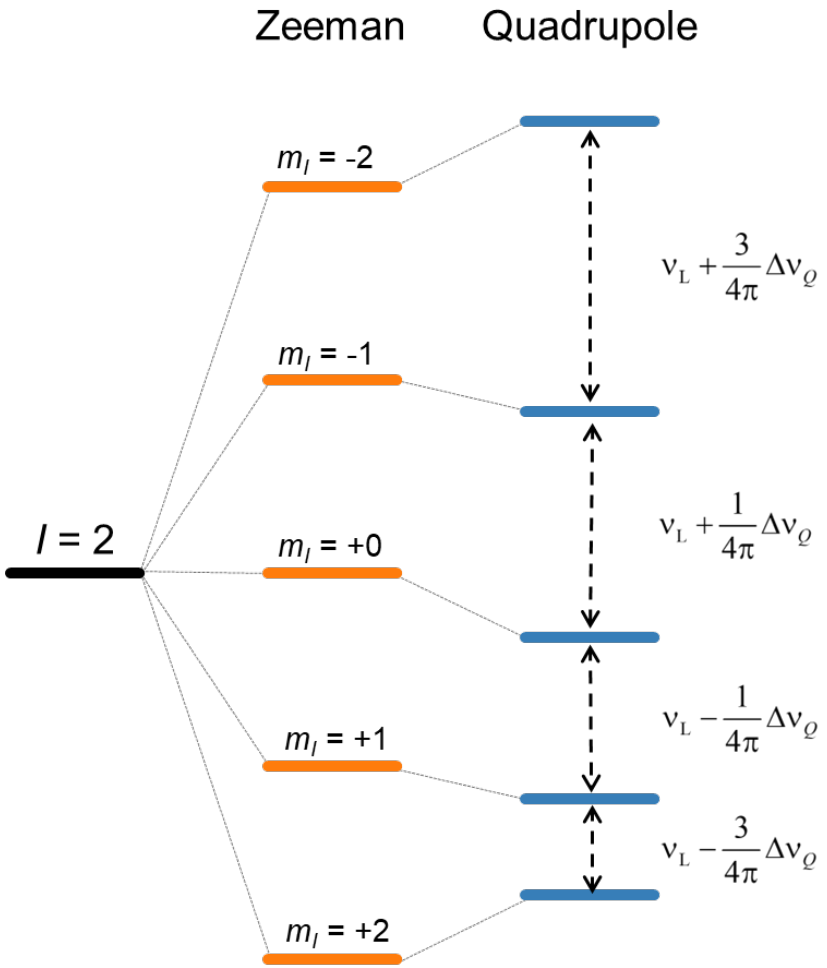

$^8Li^+$

τ = 1.2 s

(1) The quantum system has discrete, resolvable energy levels.

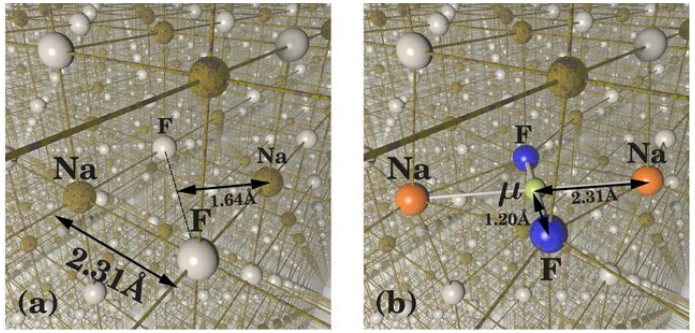

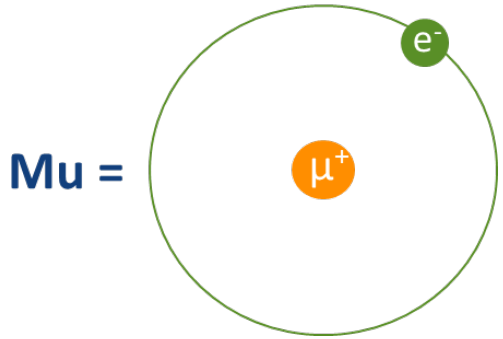

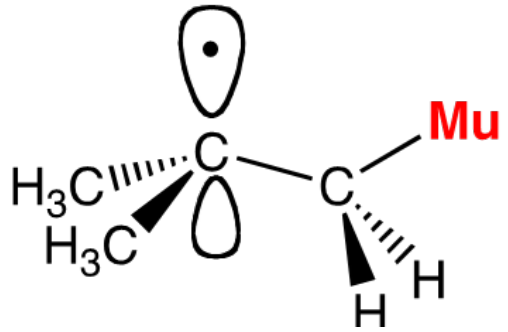

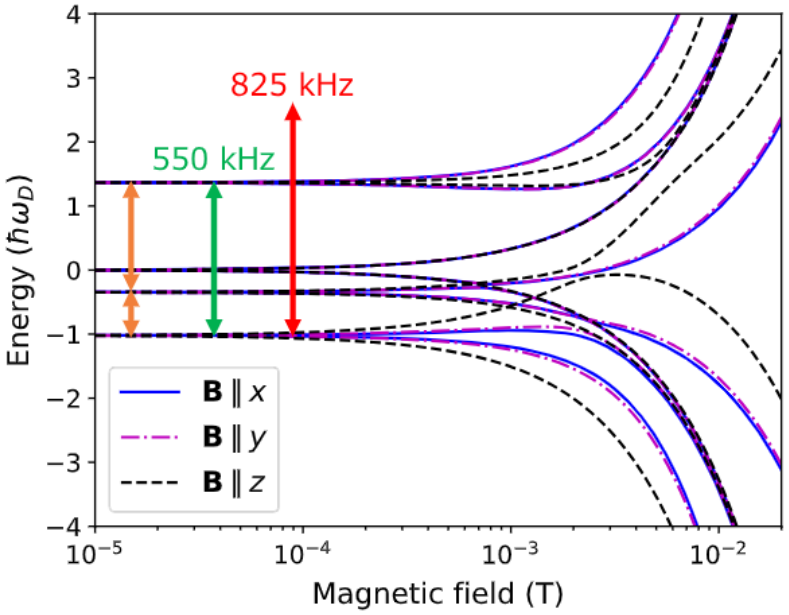

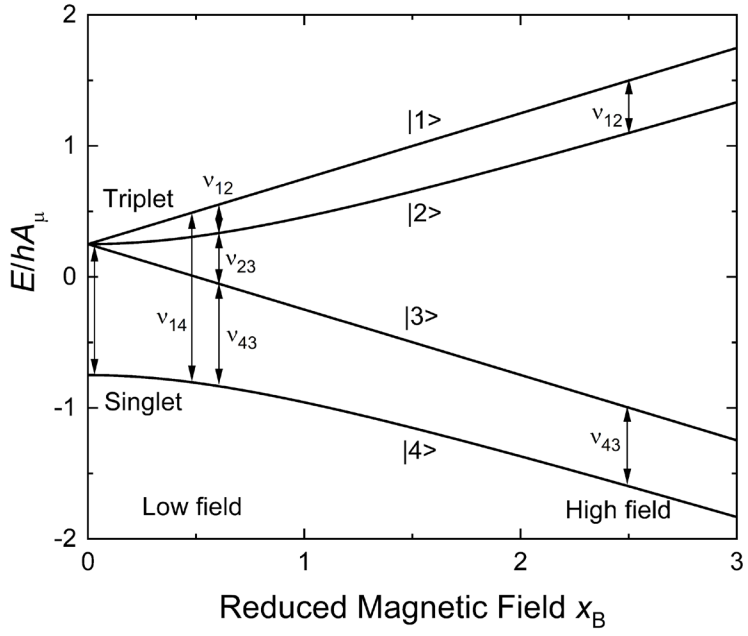

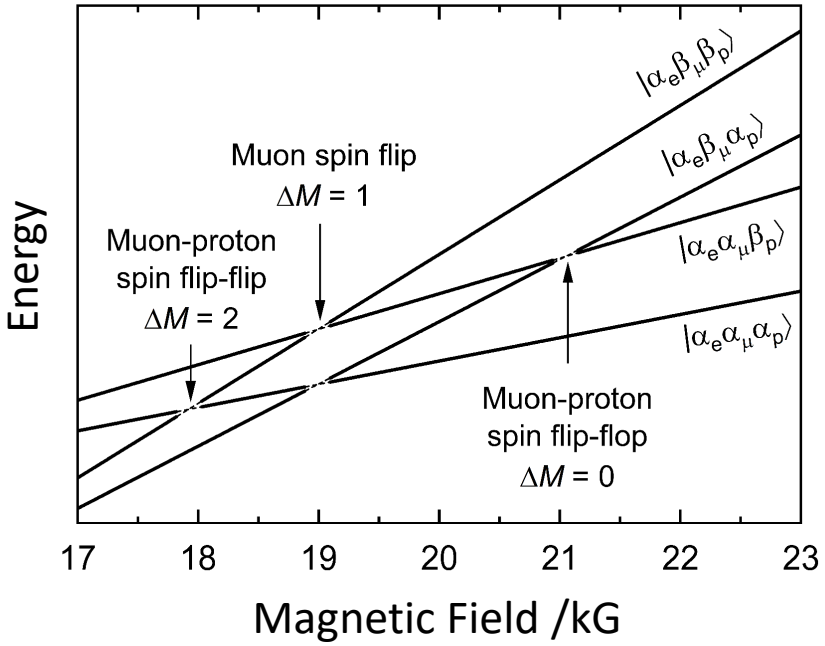

F–Mu⁺–F

Muonium

Muoniated radicals

(2) It must be possible to initialize the quantum system into a well-known state and to read out its state.

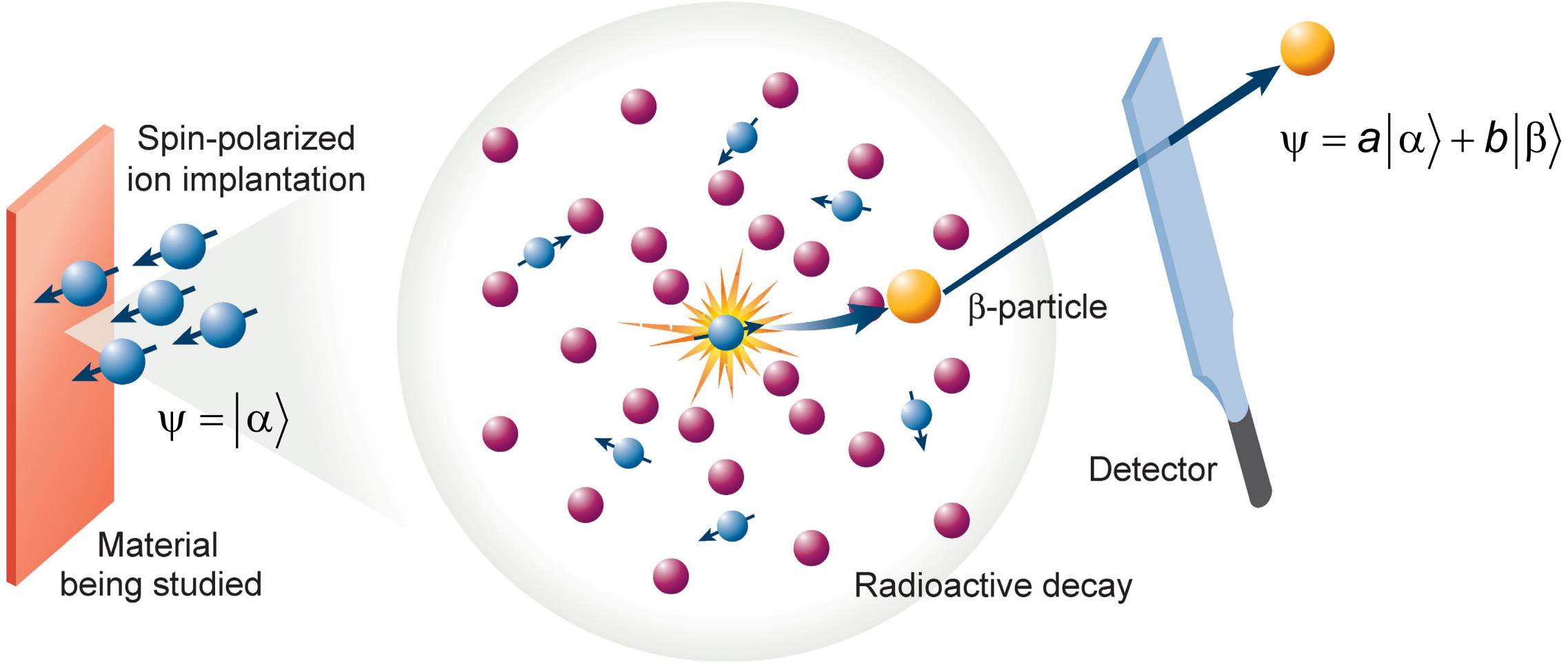

(3) The quantum system can be coherently manipulated, typically by time-dependent fields.

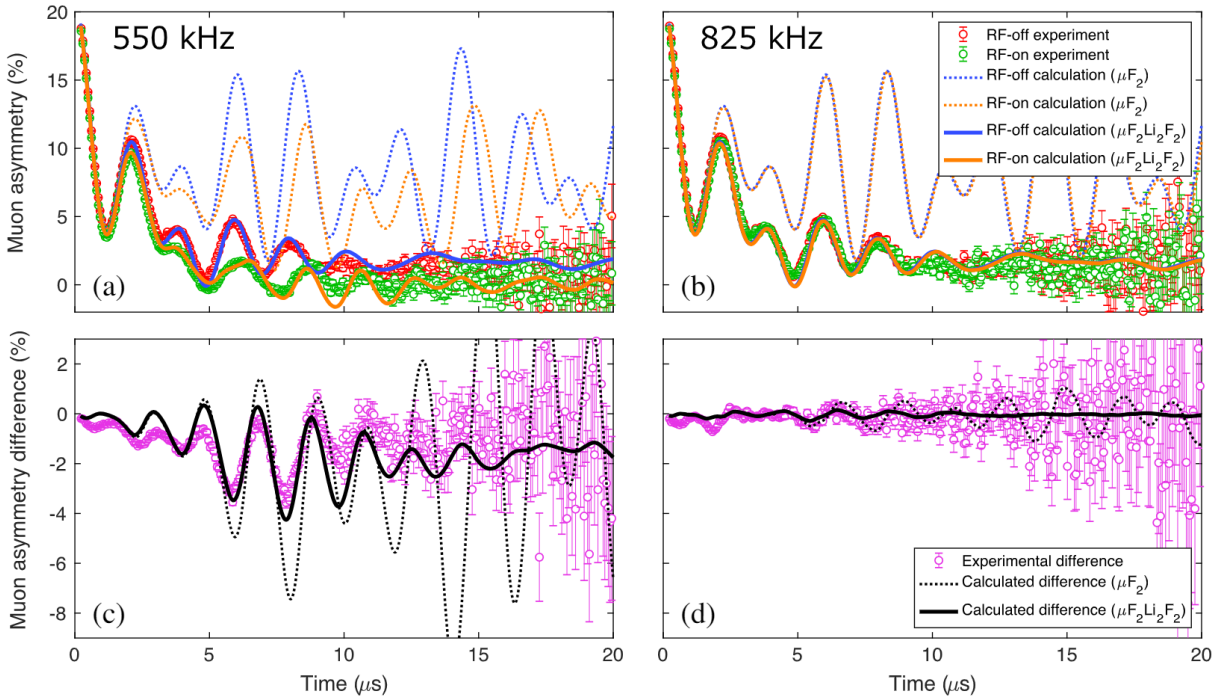

μSR of F–Mu⁺–F

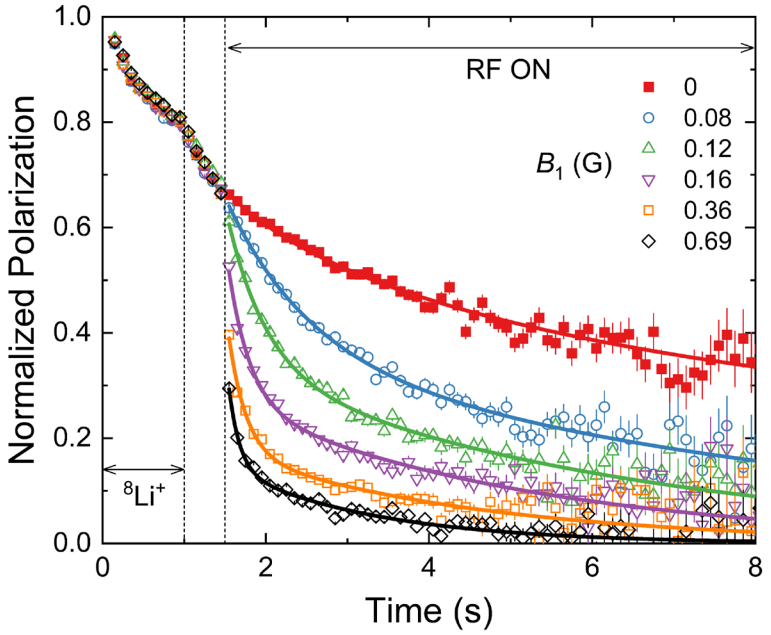

β-NMR of $^8Li^+$ in PS

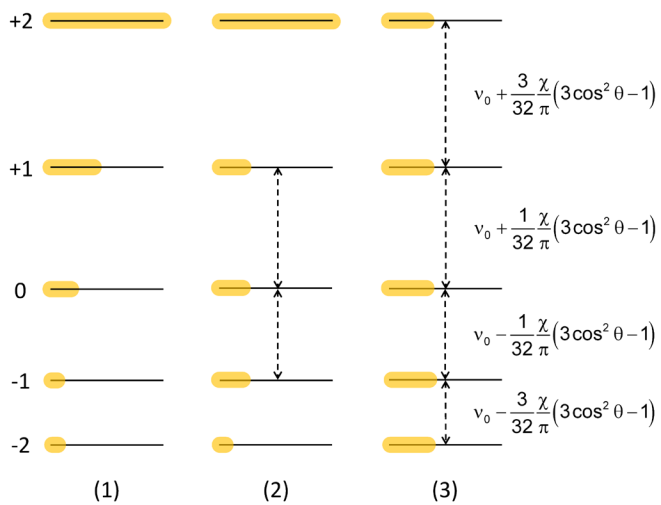

(4) The quantum system interacts with a relevant physical quantity, such as an electric or magnetic field.

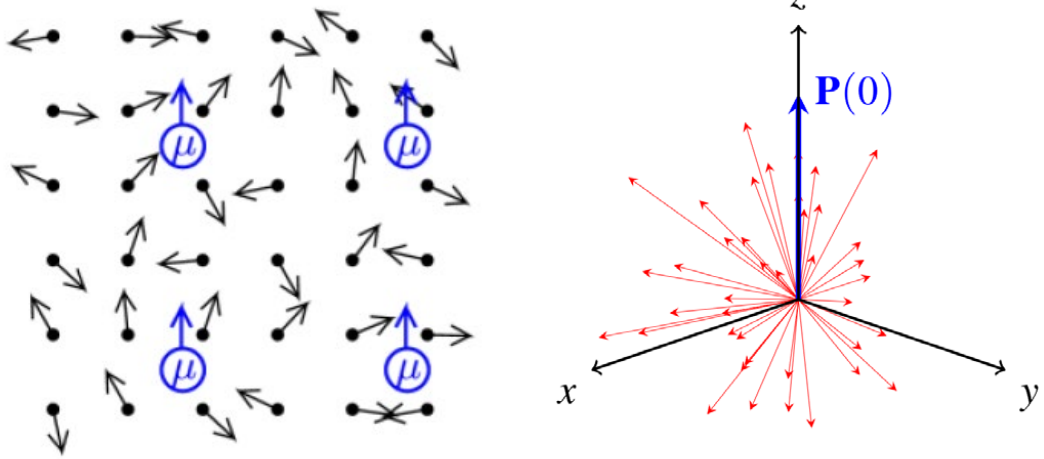

Dynamics of magnetic moments

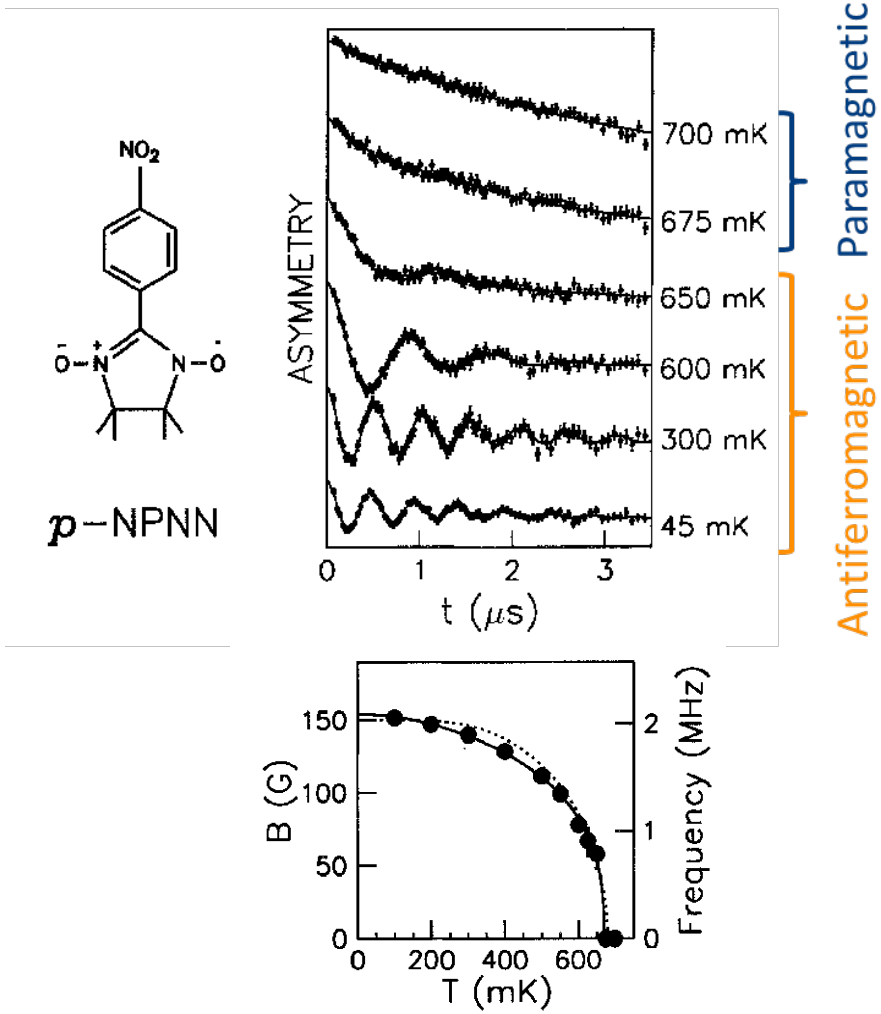

Magnetic ordering

(4) The quantum system interacts with a relevant physical quantity, such as an electric or magnetic field.

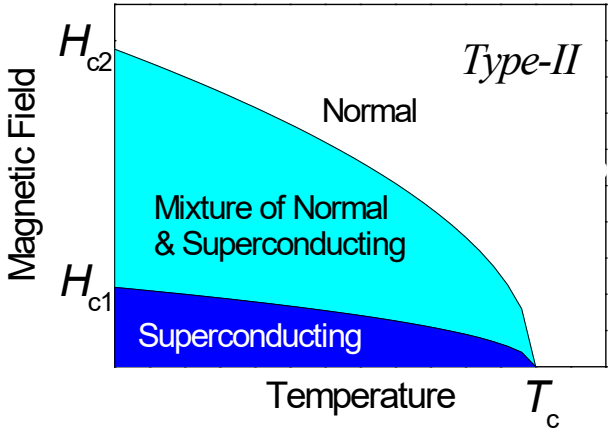

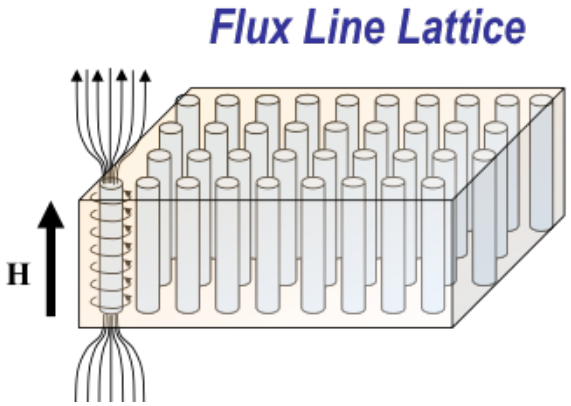

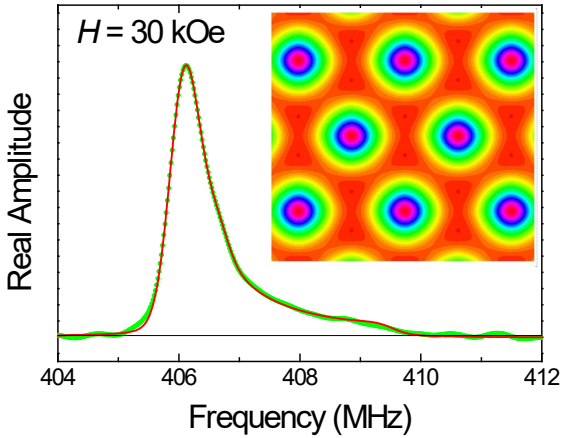

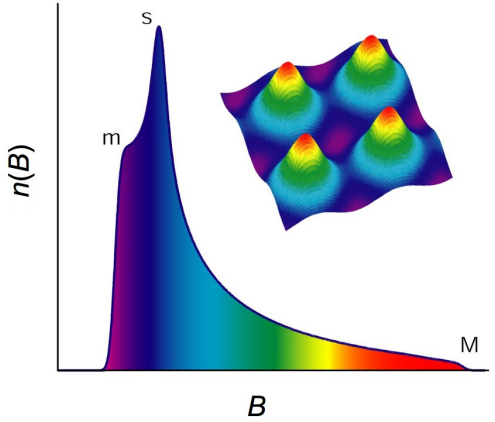

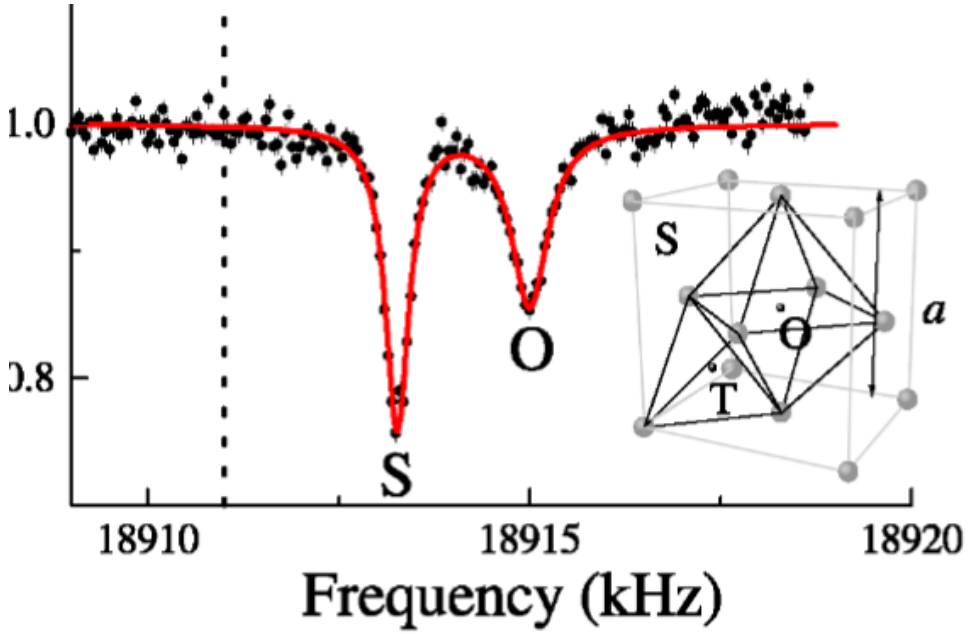

Local magnetic fields

Depth-Resolved Measurements with β-NMR

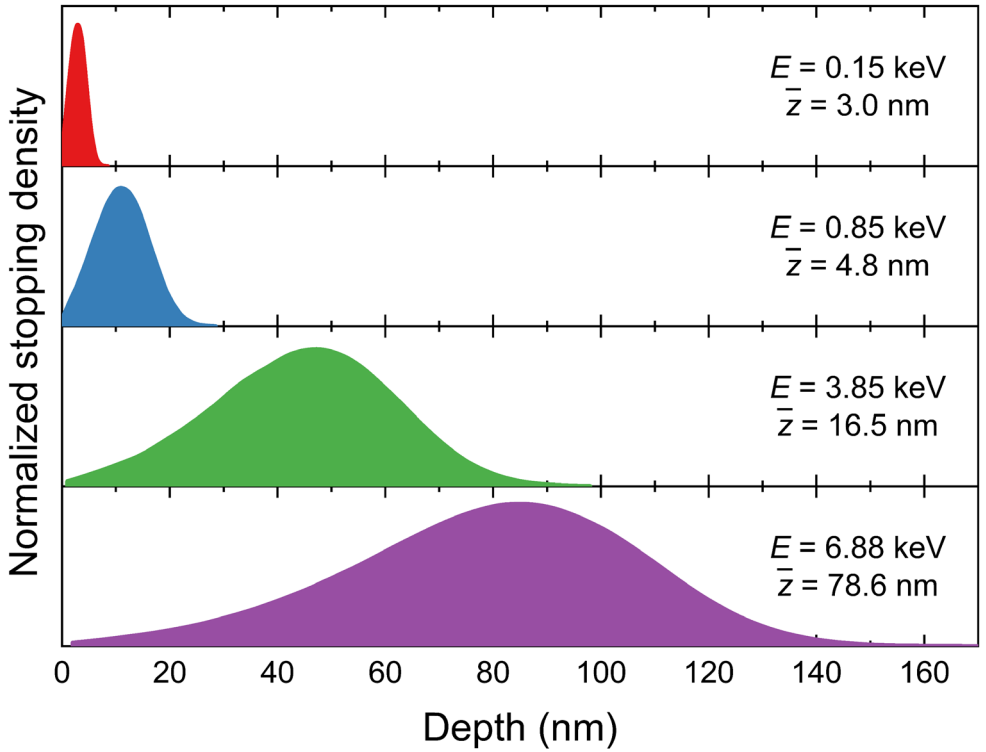

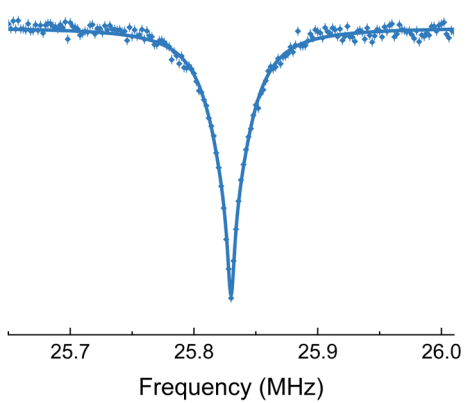

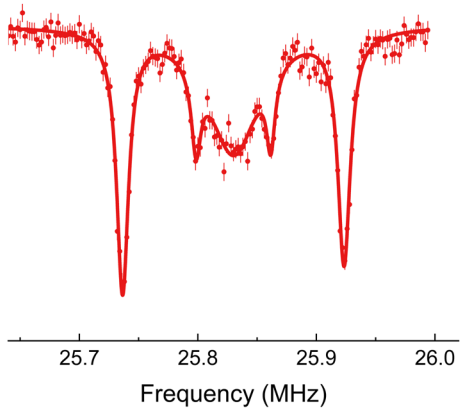

$^{8}Li^{+}$

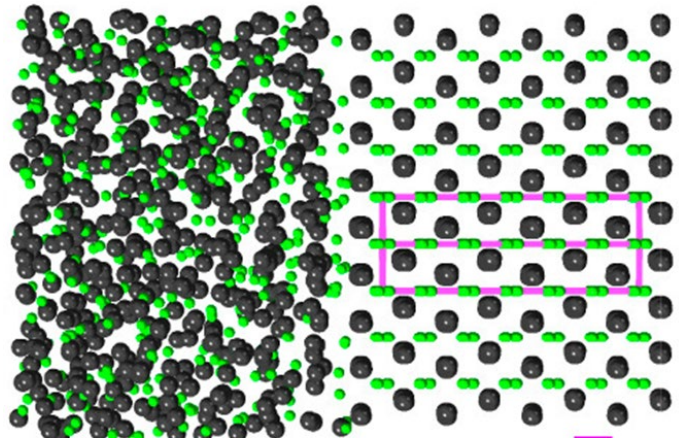

Al_2O_3

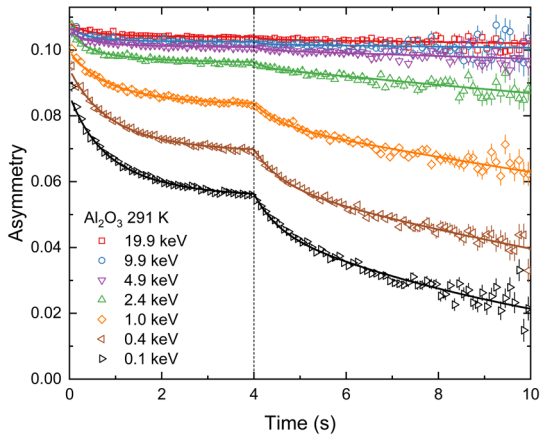

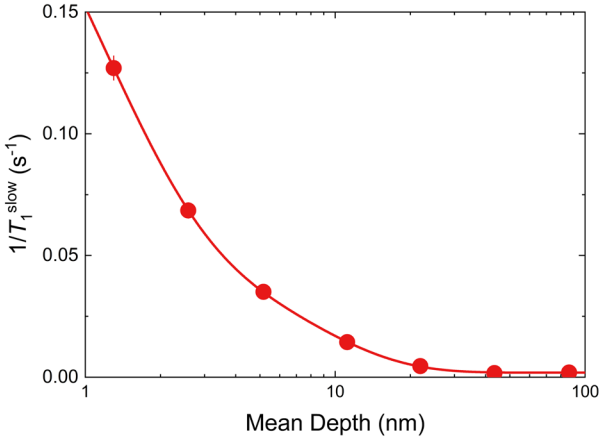

PHYSICAL REVIEW APPLIED **19,** 014032 (2023)

Material Effects on Electron-Capture Decay in Cryogenic Sensors

Amit Samanta,[1] Stephan Friedrich,[1] Kyle G. Leach,[2] and Vincenzo Lordi[1,*]

[1] *Lawrence Livermore National Laboratory, 7000 East Avenue, Livermore, California 94550, USA*
[2] *Colorado School of Mines, 1500 Illinois Street, Golden, Colorado 80401, USA*

(Received 5 June 2022; accepted 14 November 2022; published 10 January 2023)

Several current searches for physics beyond the standard model are based on measuring the electron-capture (EC) decay of radionuclides implanted into cryogenic high-resolution sensors. The sensitivity of these experiments has already reached the level where systematic effects related to atomic state energy changes from the host material are a limiting factor. One example is a neutrino mass study based on the nuclear EC decay of ^{7}Be to ^{7}Li inside cryogenic Ta-based sensors. To understand the material effects at the required level, we use density-functional theory to model the electronic structure of lithium atoms in different atomic environments of the polycrystalline Ta absorber film. The calculations reveal that the Li 1*s* binding energies can vary by more than 2 eV due to insertion at different lattice sites, at grain boundaries, in disordered Ta, and in the vicinity of various impurities. However, the total range of Li 1*s* shifts does not exceed 4 eV, even for extreme amorphous disorder. Furthermore, when investigating the effects on the Li 2*s* levels, we find broadening of more than 5 eV due to hybridization with the Ta band structure. Material effects are shown to contribute significantly to peak broadening in Ta-based sensors that are used to search for physics beyond the standard model in the EC decay of ^{7}Be, but they do not explain the full extent of observed broadening. Understanding these in-medium effects will be required for current- and future-generation experiments that observe low-energy radiation from the EC decay of implanted isotopes to evaluate potential limitations on the measurement sensitivity.

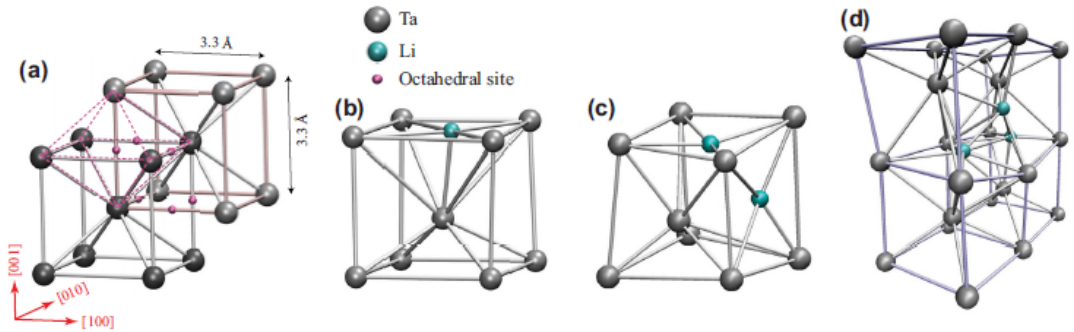

FIG. 2. (a) Bulk Ta has a bcc crystal structure, which is comprised of two intertwined simple cubic lattices, where the corner of one cube is the body center of the other. There are six octahedral interstitial sites per unit cell, which lie at the centers of each face and edge of the cubes; several representative sites are indicated by the small magenta balls. Bcc Ta with (b) one, (c) two, and (d) three clustered Li interstitials are favorable structures, with the associated local lattice distortions shown. (Only portions of the computational supercells are shown for clarity.)

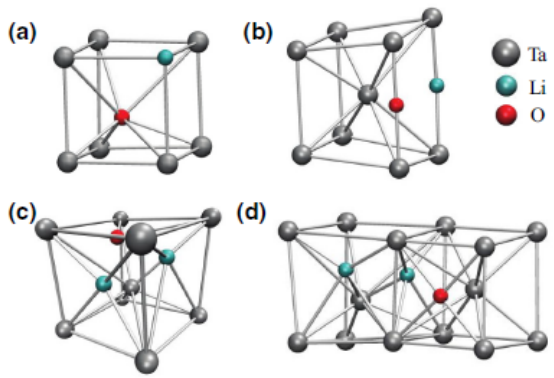

FIG. 6. Representative structures containing an O impurity near implanted Li, showing the local lattice distortions. (a) Li and O on neighboring substitutional sites, (O,1,1,*s*), or row 23 in Fig. 5; (b) Li and O on neighboring interstitial sites, (O,1,*i*,*i*), or row 18 in Fig. 5; (c) Li interstitial dumbbell with neighboring O interstitial, (O,1,*i*,2), or row 19 in Fig. 5; (d) Li interstitial dumbbell with neighboring O interstitial, (O,1,*i*″,2), or row 21 in Fig. 5. (Only portions of the computational supercells are shown for clarity.)

Applications in Non-Quantum Materials: Hydrogen Defects in Semiconductors

CdS

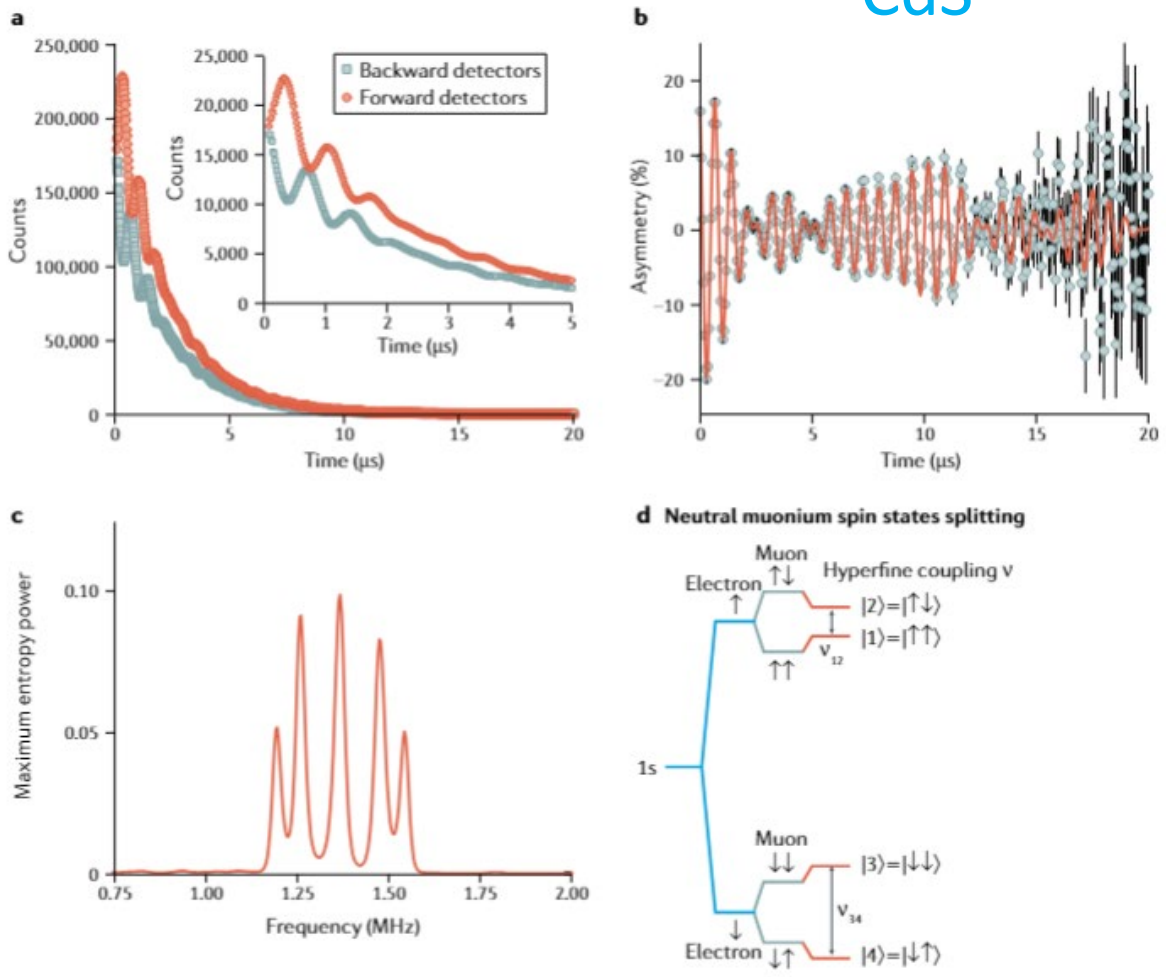

GaAs

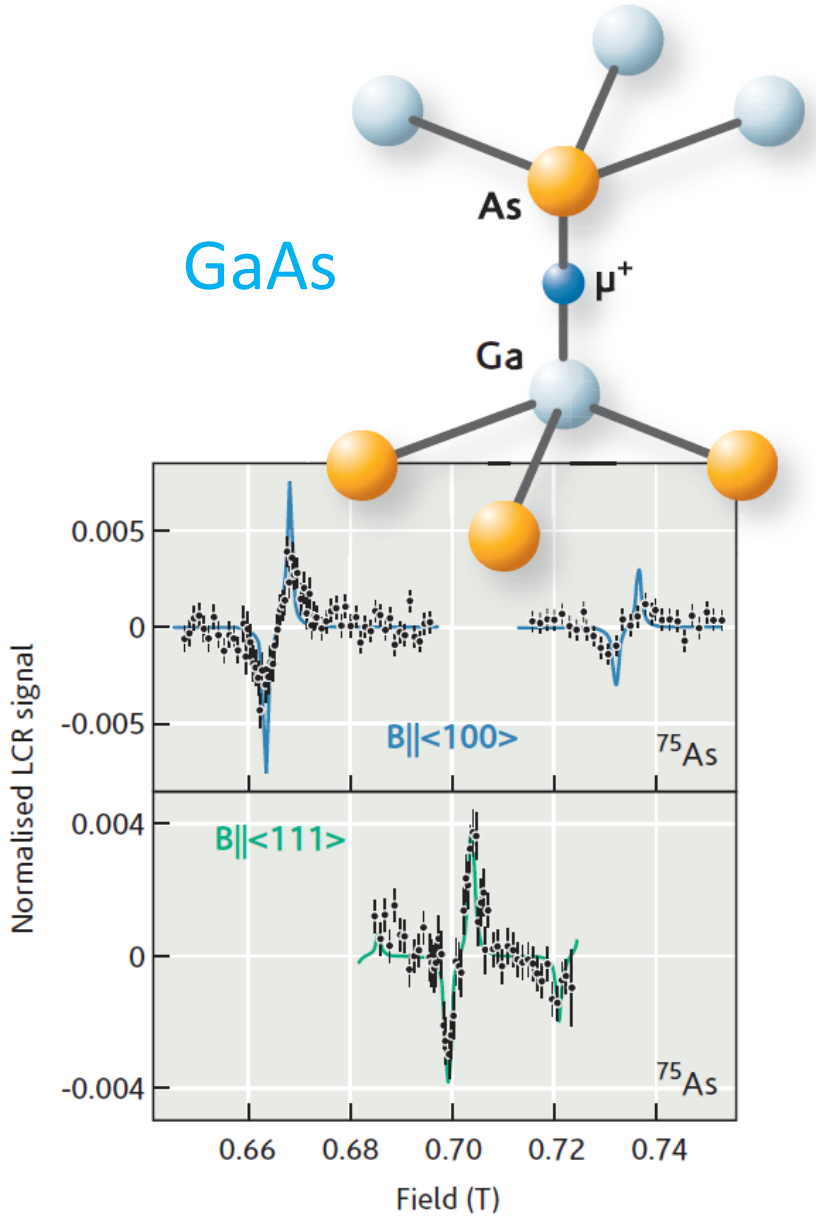

TRIUMF 20 Year Vision

A world-class accelerator centre driving use-inspired research – from the life sciences to quantum and green technologies

Leveraging our unique infrastructure to pursue research in Canada that will change the world

Green Technologies

Promising research opportunities include energy production and storage (in applications for nuclear power, batteries, and hydrogen storage); efforts to reduce greenhouse gas emissions; and leveraging of green chemical processes...

Life Sciences

New research avenues that use our technical capabilities for groundbreaking biochemistry applications and the development of pharmaceuticals will accelerate the translation from bench to bedside.

Applications in Non-Quantum Materials: Lithium-Ion Batteries

Rattling of $^8Li^+$ within one cage

Low temperature

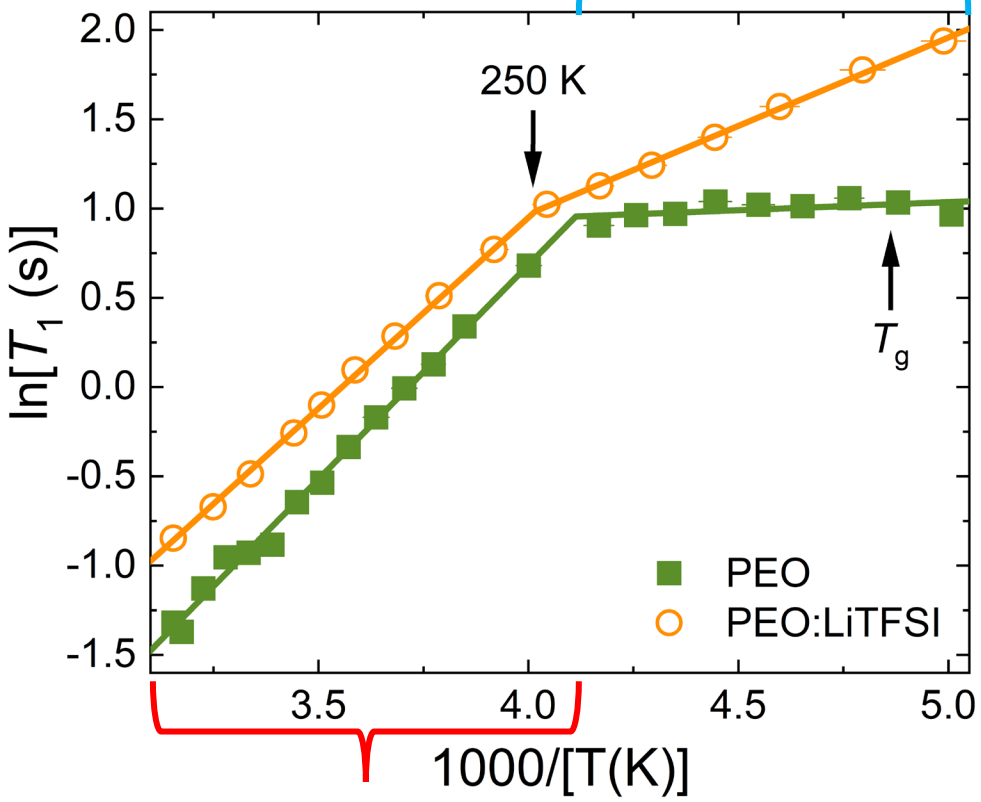

High temperature

Hopping of $^8Li^+$ between cages

Slope $\propto E_a$

Intercept $\propto \tau_0$

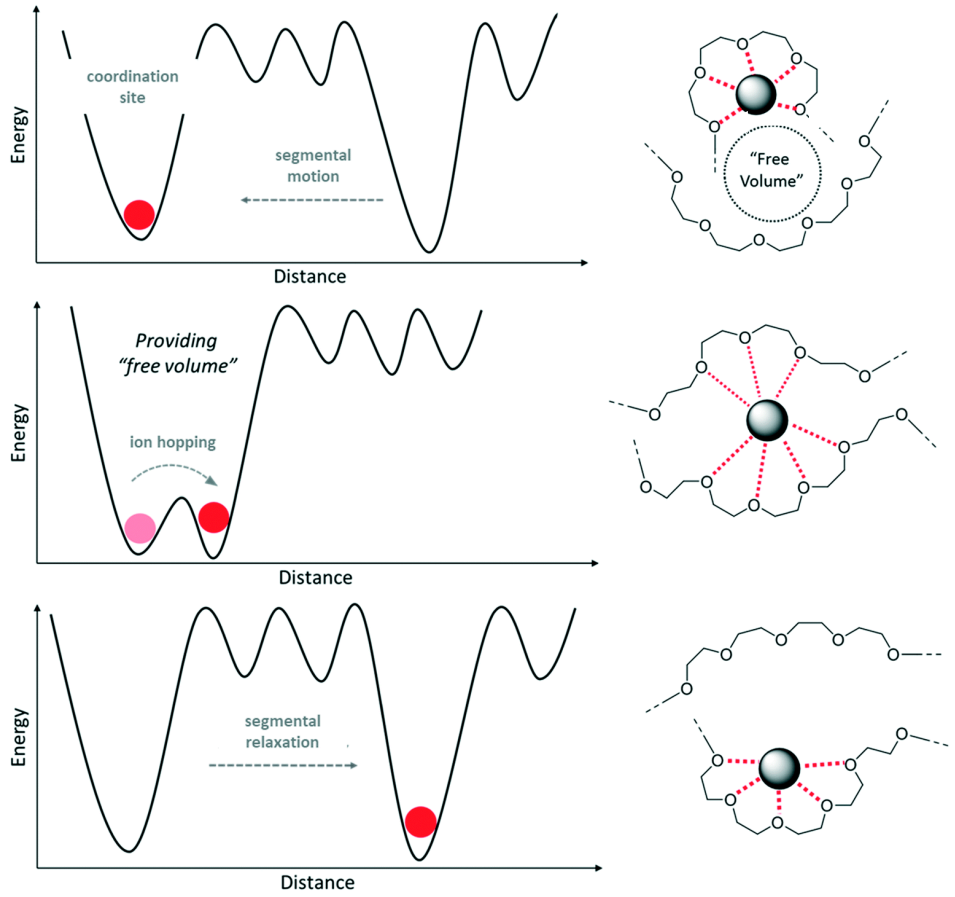

Applications in Non-Quantum Materials: Hydrogen Storage in β-Voltaic Devices

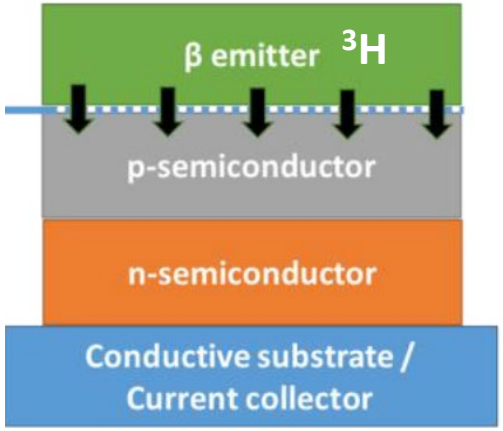

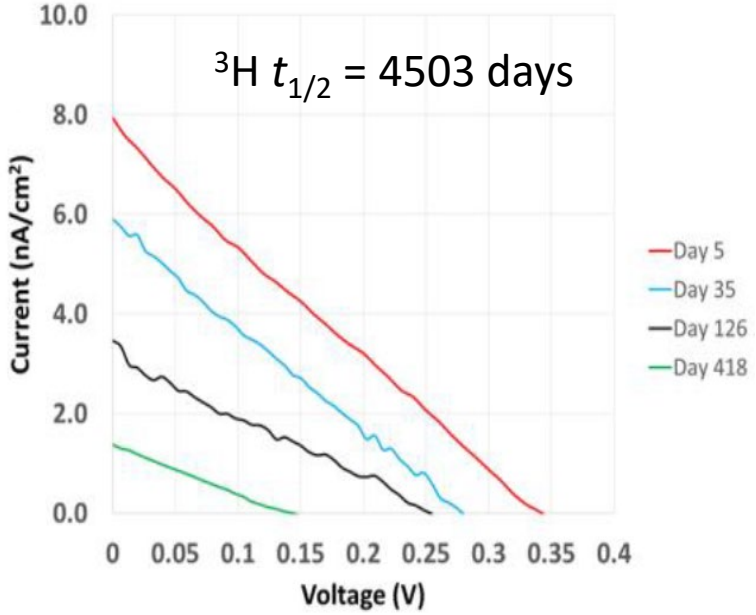

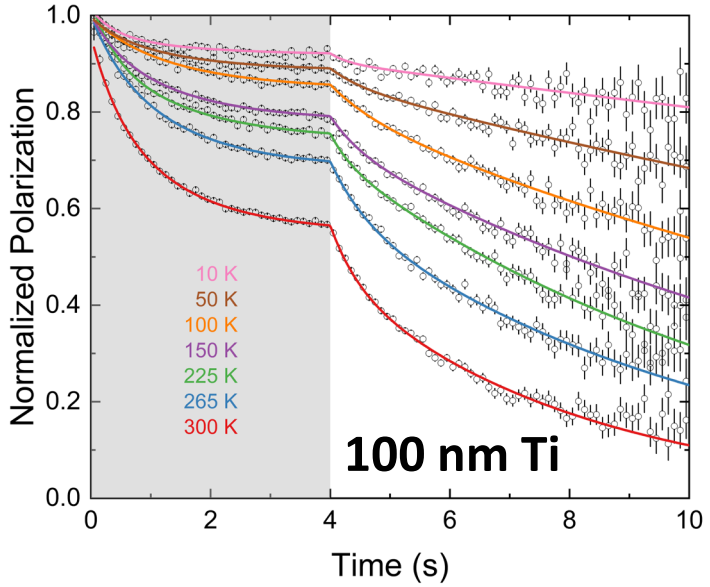

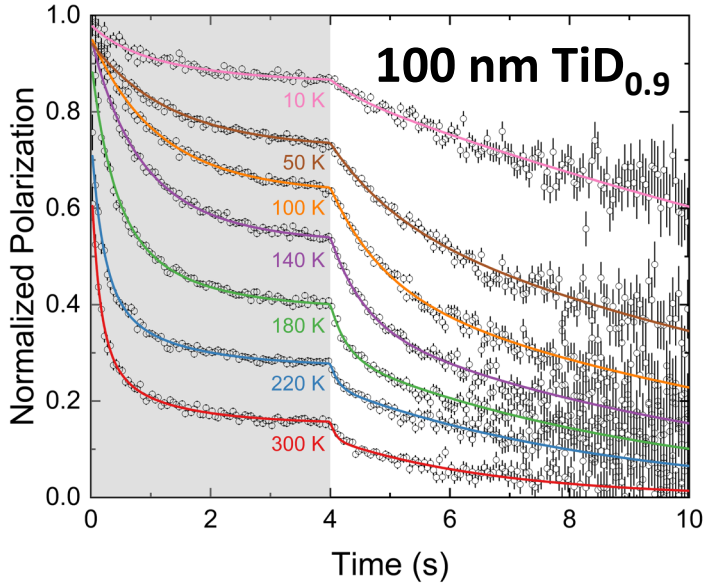

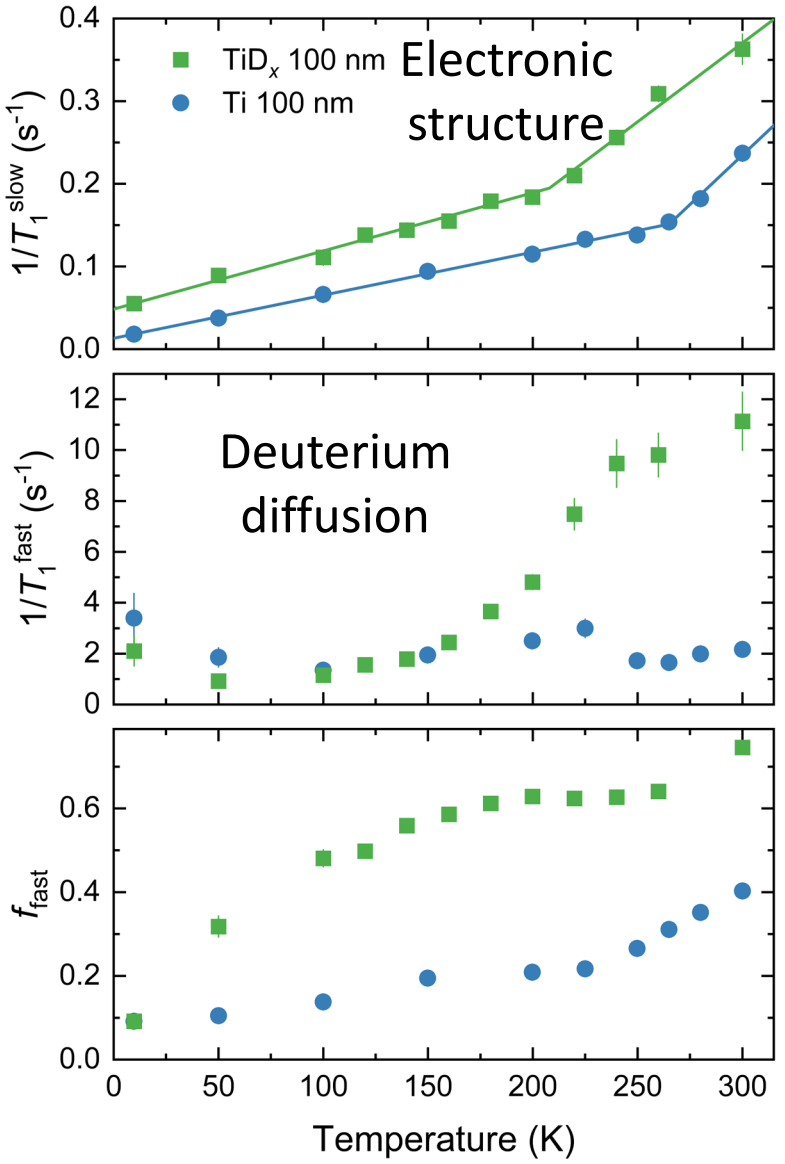

Applications in Non-Quantum Materials: Tracking Drug Molecules

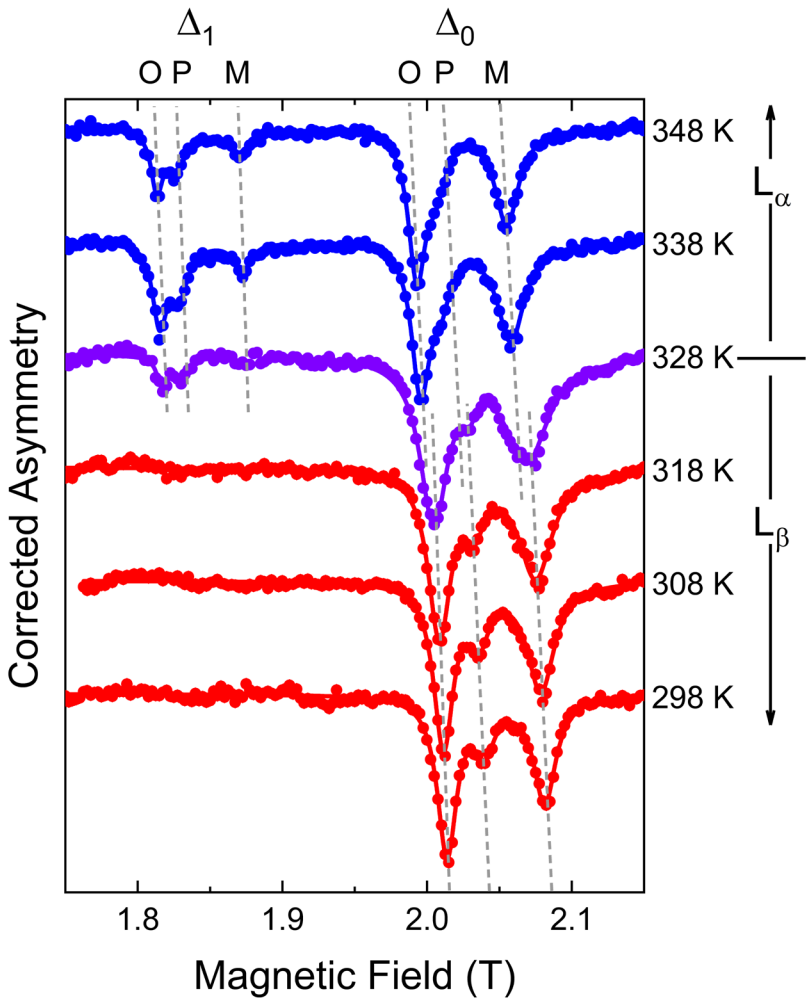

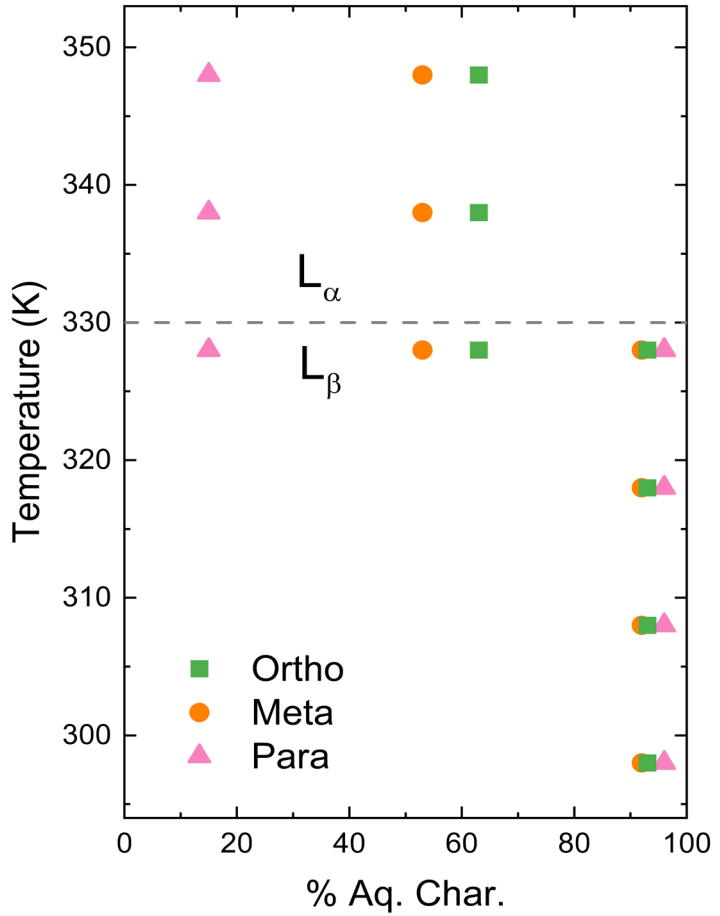

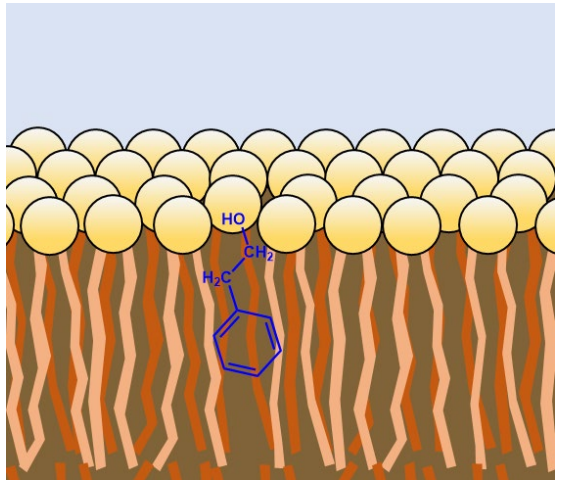

High T
L_α fluid
phase

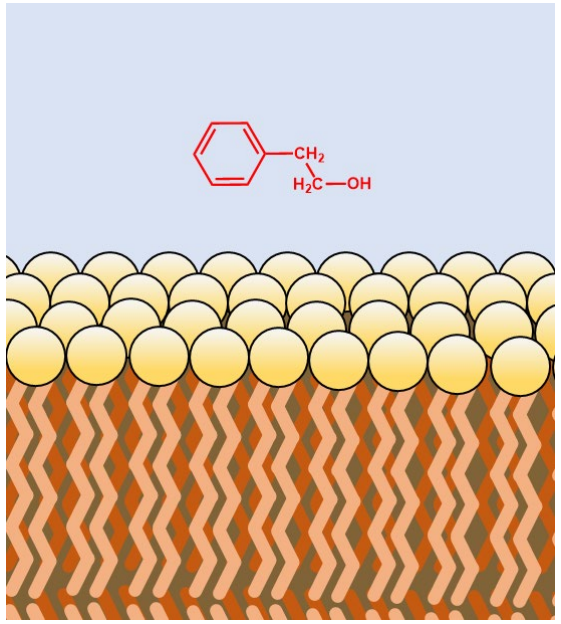

Low T
L_β gel
phase

µSR Beamlines

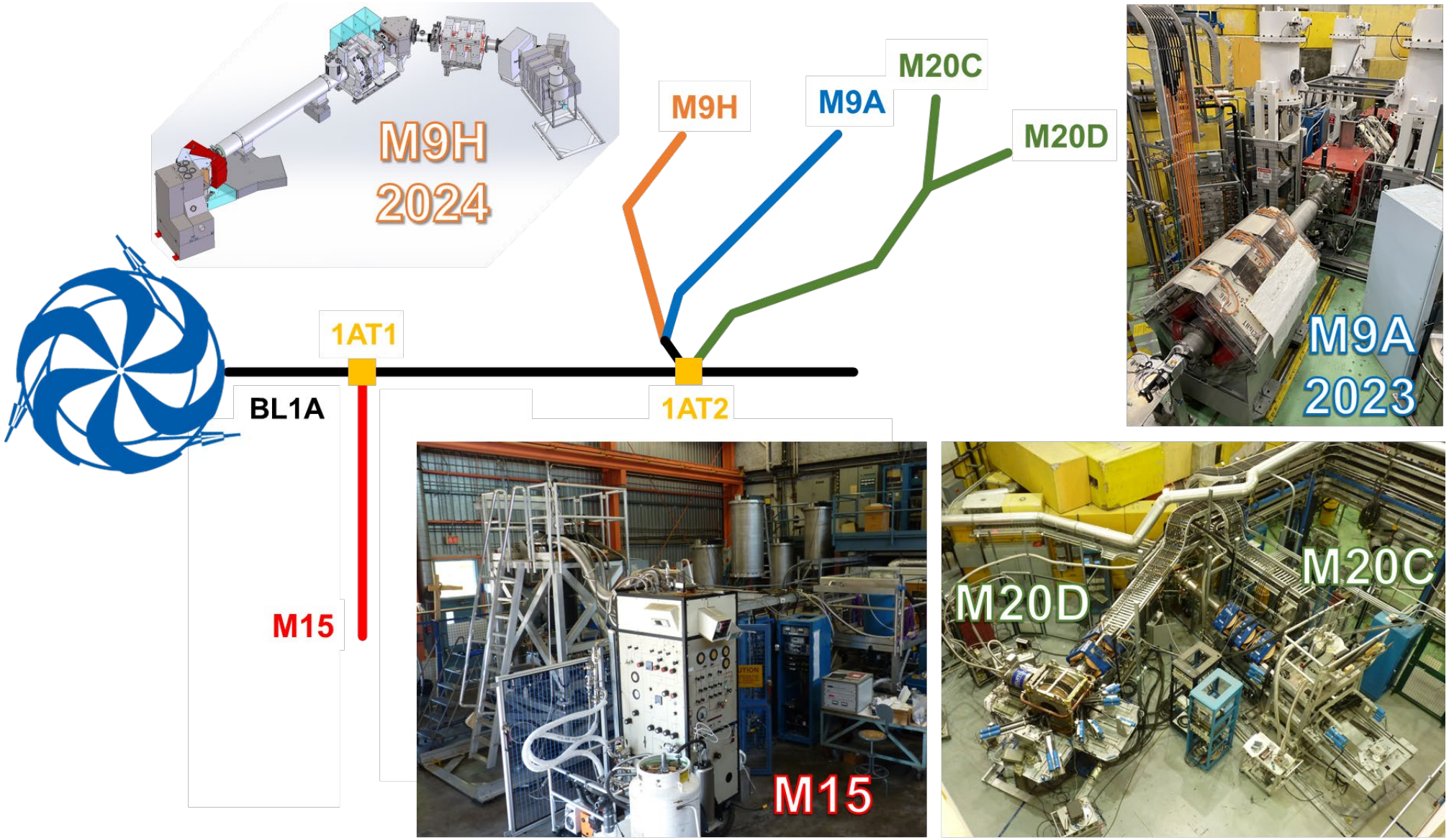

μSR Spectrometers

LAMPF

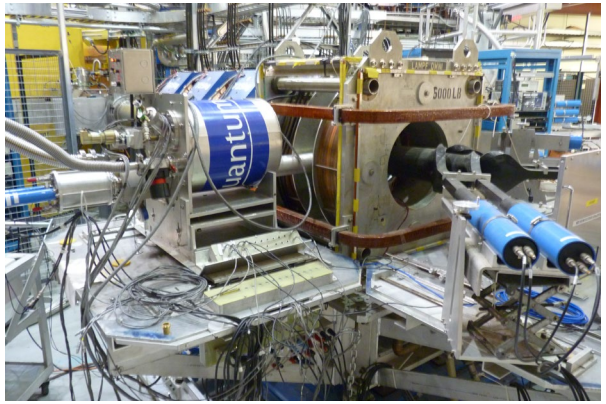

- 4 x Helmholtz
- 0.3 T / *z*, 10 mT / *x*, *y*
- Miss Piggy: 1.7 – 330 K
- Gas flow: 2.8 – 330 K
- Oven: 290 – 900 K

NuTime

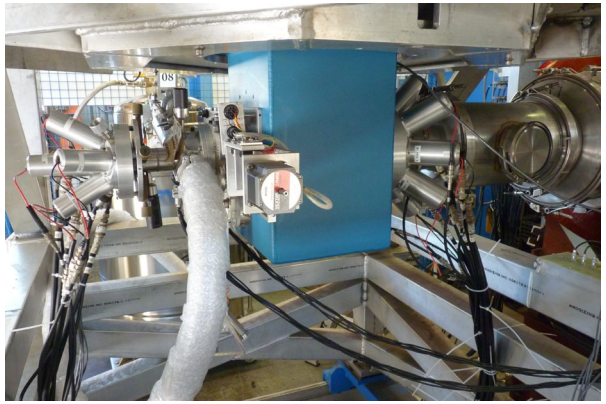

- Superconducting Solenoid
- 7.0 T / *z*
- ^{4}He cryostat: 2 – 330 K

DR

- Superconducting Helmholtz
- 5 T / *z*, 2.5 mT / *x*
- 15 mK to 10 K

Helios

- Superconducting Solenoid
- 6 T / *z*, 2 mT / *y*
- Circulator: 250 – 475 K
- Gas flow: 2.8 – 330 K
- Oven: 290 – 900 K

β-NMR Spectrometers

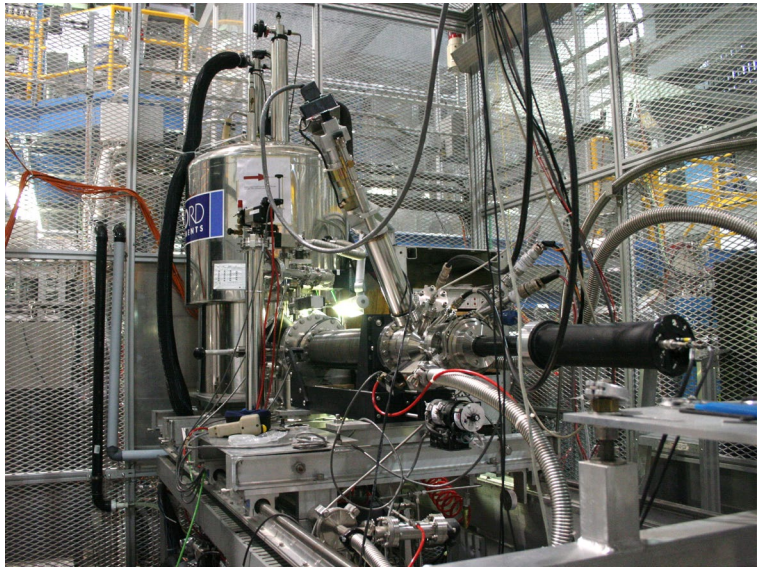

βNMR

- Maximum magnetic field: 9 T
- Maximum magnetic field with RF: 6.55 T
- Temperature: 4 – 320 K

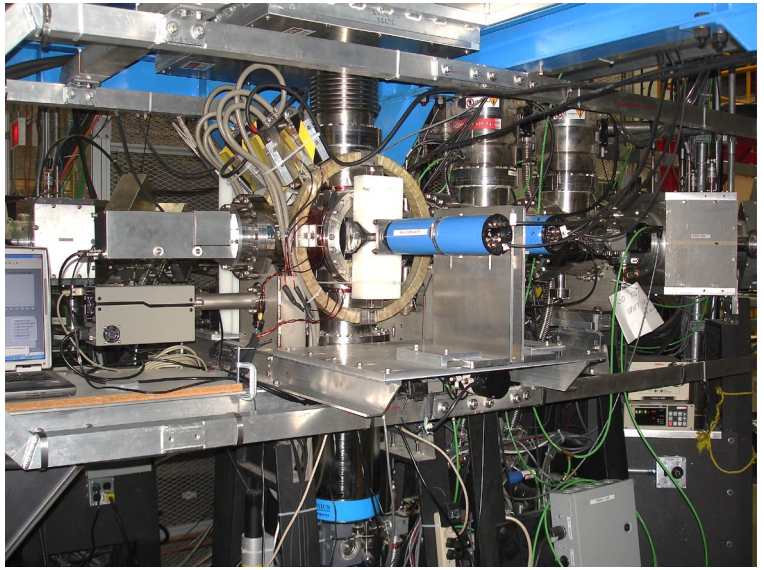

Low-field βNQR

- Magnetic field: 0 – 24 mT
- Normal cryostat: 4 – 320 K
- Cryo-oven: 4 – 400 K

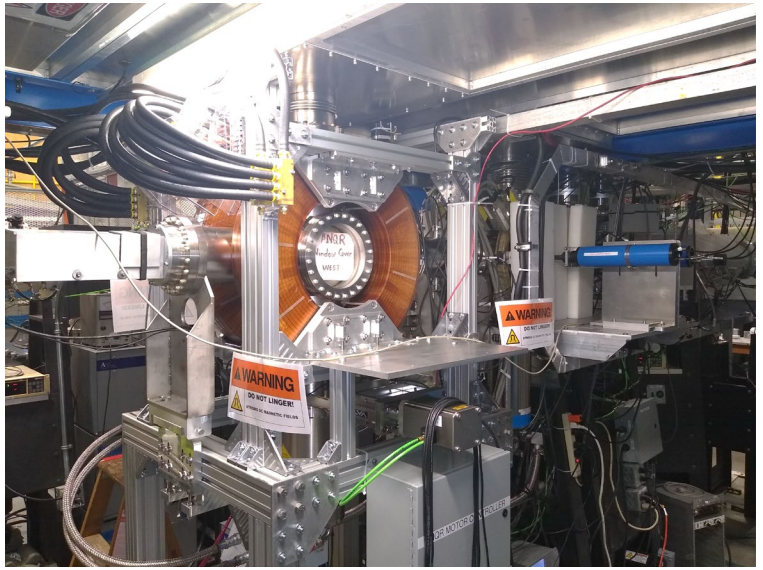

Mid-field βNQR

- NSERC RTI funded + TRIUMF contribution
- Commissioned 2022
- Magnetic field: 0 – 0.2T
- Cryo-oven: 4 – 400 K

Non-Destructive Elemental Analysis with Negative Muons

MIXE (Muon Induced X-ray Emission)

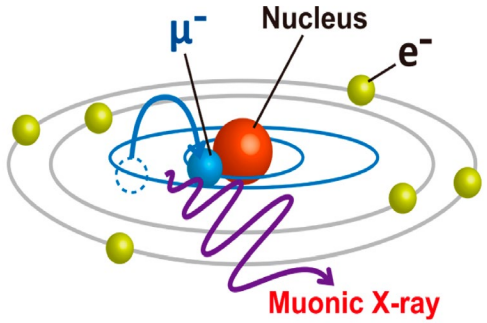

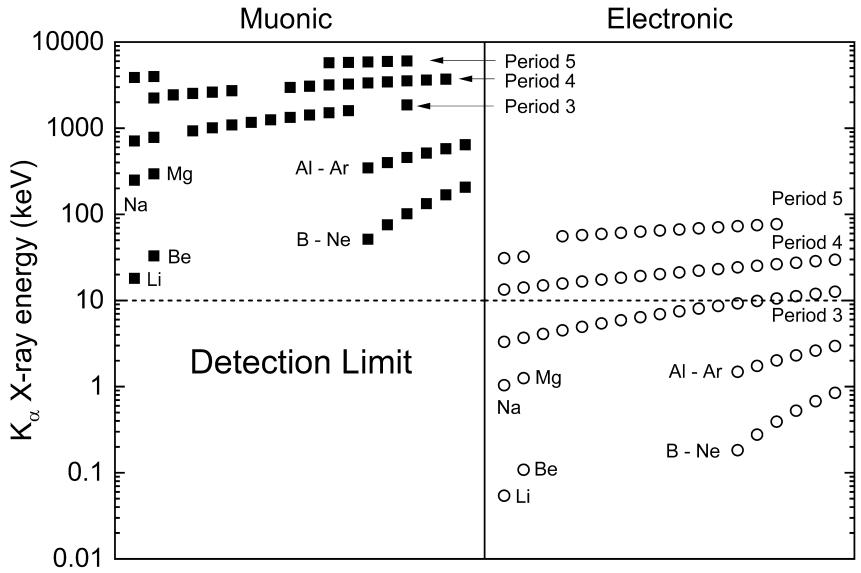

Muon Lifetime and μ⁻SR